Magnetometer Measurement of the main kick pulse and eddy currents transient magnetic field in g-2 experiment at Fermilab

Nicolò Rossolino

Università Degli Studi di Napoli Federico II, Naples, Italy
Supervisors: Marco Incagli, Hogan Nguyen, Anna Driutti

Abstract

In the framework of the Standard Model(SM) theory, Dirac equation predicts for the muon giromagnetic factor $g = 2$, but the Quantum Eletrodynamics, Electroweak and Hadronic corrections add $\sim 10^{-3}$ to the value of g. The $g - 2$ experiment aims to measure the "muon anomalous magnetic moment" $a_\mu = \frac{g-2}{2}$ with a precision of 140 ppb in order to probe the Standard Model and search for new physics.

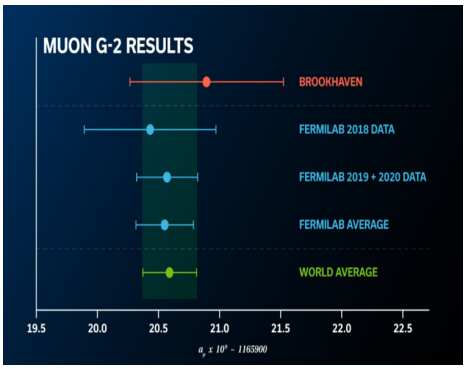

Figure 1: The latest results of the Muon $g - 2$ experiment

From Figure 1 it is possible to see the experimental results obtained so far. In this report I will present my work on the magnetometer measurement of the main kick pulse and the transient magnetic field generated by the eddy currents, performed at the Muon $g - 2$ experiment at Fermilab.

1 Introduction of the experiment

The Muon $g-2$ experiment involves capturing and storing muons in a magnetic field, causing them to precess like gyroscopes. A 3.1 GeV muon beam is injected into a 14 m diameter storage ring (SR), where both muon's spin and momentum vectors precede. The difference between the spin frequency and the cyclotron frequency called "anomalous precession frequency" is related to a_μ through $\omega_a = a_\mu \frac{q}{m} B$, where B is the magnetic field inside the SR. Hence a_μ can be extracted by accurately measuring ω_a and B. Figure 2 shows the injection and the storage process of muons. While in the Figure 3 it is possible to locate the Muon g-2 kicker system which my work at Fermilab was focused on.

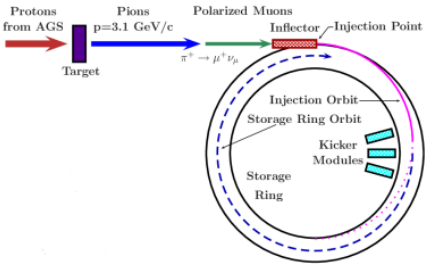

Figure 2: Schematic of the muon injection into the $g-2$ Storage Ring, The blue dashed line represents the "magic radius" orbit. See text for more details.

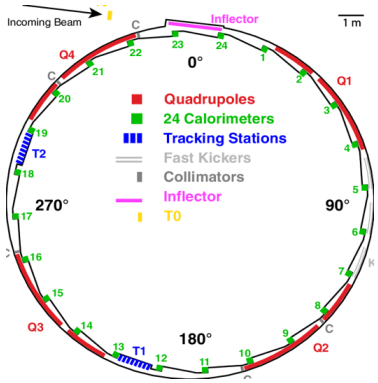

Figure 3: Main components of the $g-2$ Storage Ring.

The kicker system is needed since when the muons enter the ring, they need to be centered into stable orbit, which radius is called "magic radius" (R_0 in the following parts of the report) before starting to properly turn. In order to accomplish this, three kickers produces a 200-300 Gauss magnetic field that "kicks" the muon beam on the orbit R_0 as shown in Figure 2.

2 G-2 kicker system

The kicker system is composed by three 1.27 m long non-ferric aluminum electromagnets, placed a quarter of the ring circumference from the inflector and they are pulsed with ~ 4 kA. These are localized pulses with the effect of "kicking" the muons onto a stable orbit. Non-ferric materials were used to not affect the a_μ measurement, because it is sensitive to magnetic field variations. The train of muons is divided in two groups and separated in time by 200ms, each group is then further splitted in 8 bunches injected in the ring every 10 ms, as shown in Figure 4.

Figure 4: Schematic of the muon injection time.

Each bunch is 120ns long, and it takes about 149.2 ns to complete an entire turn of the ring. The kicker operated during the full duration of each beam bunch and ceases before the muons make one full revolution of the ring. To address these timing specifications, the blumlein system works like a capacitor where the charge-discharge phenomenon happens in a short time.

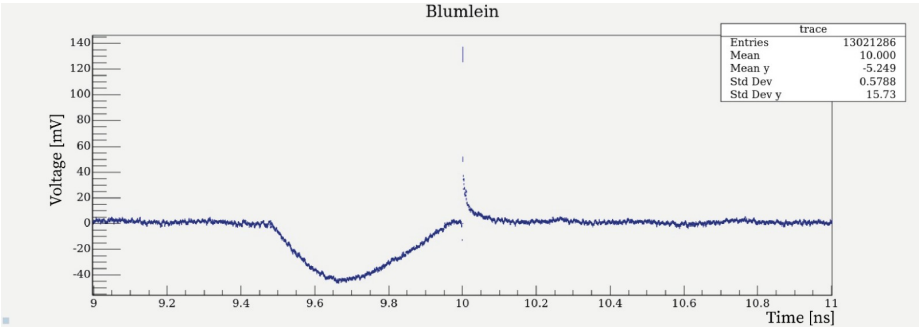

Figure 5: Blumlein charge-discharge phenomenon: the charge process (represented by the negative bump) starts around 9.4 μs and last for about 0.6 μs. The discharge, *i.e.*, the kicker pulse (positive spike) is much faster ($\sim$ 100 ns) and starts around 10 μs.

From the Figure 5 it is possible to see the blumlein charge starting around 9.4 μs and at the 10 μs the "kick". The kick lasts $\sim$ 100 ns and produces eddy currents that cause a transient magnetic field in the time window in which w_a is measured. Although the eddy currents generated a magnetic field which is much smaller than to the one provided by the storage ring (1.45 T) it contributes as a systematic uncertainty on the experimental results of some ppb. Since the Muon g-2 experiment is a high precision experiment and it aims to reach 140 ppb uncertainty, precisely quantify the kicker transient magnetic field is very important. This measurement is currently made at the same time by two separate teams at Fermilab. Both teams are using magnetometers based on Faraday rotation effect but with different characteristics: one uses a fiber magnetometer, while the other one uses a breadboard magnetometer.

My work at Fermilab has been done only with the breadboard magnetometer built by the INFN team.

3 Faraday Effect

The INFN magnetometer works with Faraday rotation effect, a property of dielectric crystals materials (Verdet crystals). When these crystals are placed inside magnetic field and a light beam passes inside them, the Faraday effect causes a polarization rotation of the light beam which is proportional to the projection of the magnetic field along the direction of the light propagation as shown in Figure 6.

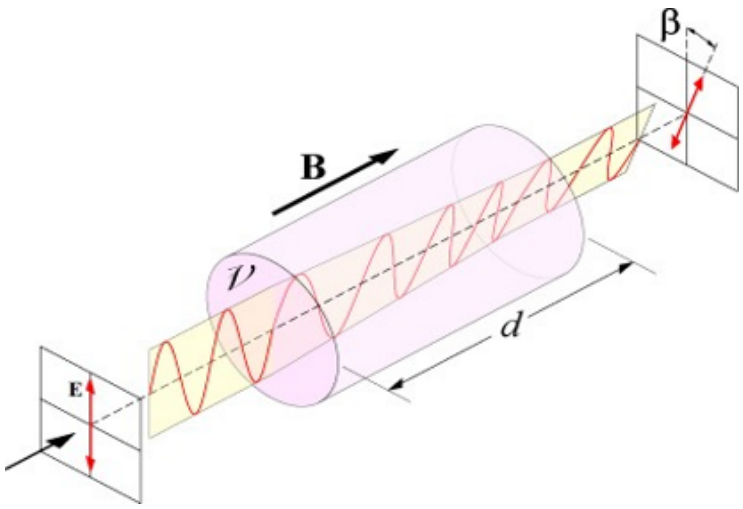

Figure 6: Faraday Rotation into a Verdet crystal, β is the rotation angle of the polarization.

The rotation is described by a linear equation: $\beta = B\,V\,d$, where β is the rotation angle, B is the magnetic field inside the crystal in the direction of the light propagation, d is the length of medium traversed where the light interacts with the magnetic field, V is the Verdet constant for the material. The latter is an empirical proportionality constant that depends on the crystal and varies with both frequency and temperature, and it is tabulated for various materials. The crystal used by the INFN magnetometer is made of Terbium Gallium Garnet (TGG), and it has a reported Verdet constant of $-131\,\mathrm{rad/(T\,m)}$. The TGG crystal has been chosen since its rotation angle is a multiple of 2π when inside 1.45 T magnetic field.

4 The Breadboard Magnetometer

Figure 7 shows the setup of the breadboard with in red depicted the laser path.

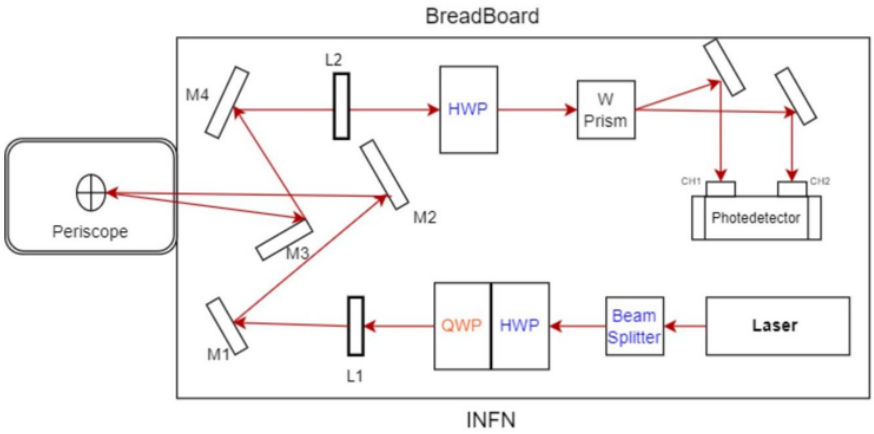

Figure 7: Schematic of the INFN breadboard magnetometer.

From the Figure 7 the laser path (in red) and the principal components of the breadboard can be seen. The main components are:

- Laser: 633 nm linearly polarized red light laser.
- Beam splitter: to split the beam in the two different polarization.
- The first Half Wave Plate(HWP): to maximize the signal once it gets out of the beam splitter.
- A Quarter Wave Plate(QWP): to study the noise (not used during this work).
- Dielectric mirrors: to deflect the beam into the periscope and into the photo-diodes.
- Periscope system: composed by two TGG crystall at different radial distances.
- Focusing lenses: with $f = 750$ mm and $f = 200$ mm.
- Second Half Wave Plate: used to balance the signal before the acquisition.
- A Wollaston Prism: used to split laser beam in two beams with a defined angles.
- Fast photo-diodes or slow photo-detector: the first one used to collect main kick signals and the second one for the eddy currents transient magnetic field signal.

Measurements were taken at two different radial distances, the first one at R_0 (the magical radius distance), and the second one at R_1, $\sim 1.5\,\text{cm}$ further from the first one thanks to a periscope system designed to allocate two Verdet crystals. A picture of the periscope system is shown in Figure 8.

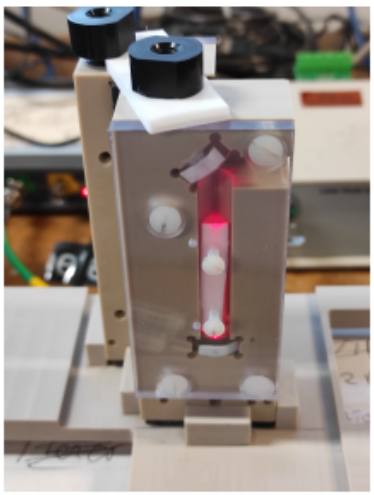

Figure 8: Picture of the periscope system.

The periscope systems comprises:

- Plastic Bridge: used to reduce the mechanical vibrations after kicks.
- Periscopes: two structures each composed by a TGG crystal inserted between two mirrors.
- Teflon bar: placed at the top to connect the two periscope: it improves the stability of the structure.

As shown in Figure 9, the laser light from the breadboard hits a first mirror at the top of a periscope, and is deflected so that goes through the TGG crystal: before hitting a second mirror, that send the light back to the first mirror going through the crystal a second time. So, in total we have two Faraday rotation. After the light is directed back to the breadboard, goes into the Wollaston prism where it is splitted in two rays each of them reaches a photo-diode. The HWP is used to set the difference between the two signals equal to 0. In this way, when the polarization changes, there will be an output different than 0.

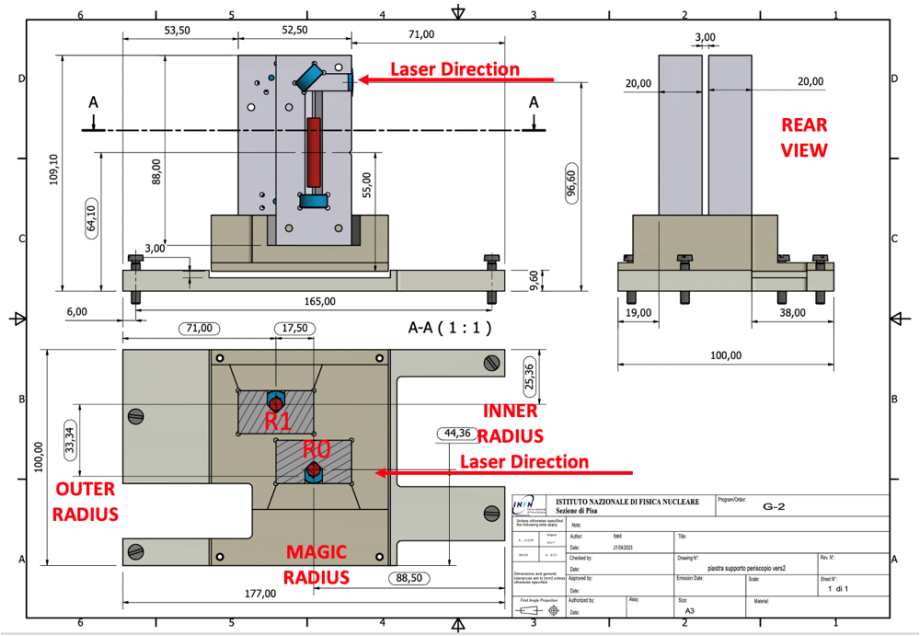

Figure 9: Details of the periscope system.

A picture of the INFN Breadboard and the periscope system with superimposed the beam path (red dashed line) described before is shown in the Figure 10.

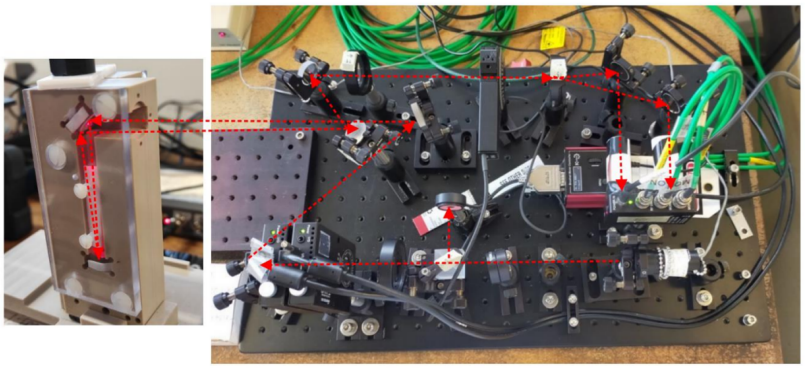

Figure 10: Picture of the breadboard and the periscopes with the beam path depicted in red.

5 Hardware Work

The preparation of the experimental setup is very important: to reach the precision goal, the reduction of the noise and of the uncertainties is fundamental.
First, with the help of two technicians the periscope system was installed in the vacuum chamber inside the kicker 3 region, between the aluminium plates: the main difficulties of this work were cause by the narrowness of the environment. Then the breadboard that was in the MC-1 building mezzanine was moved into the ring hall mounted outside the third kicker cage.
Pictures of the setup after the installation procedure are shown in Figure 11.

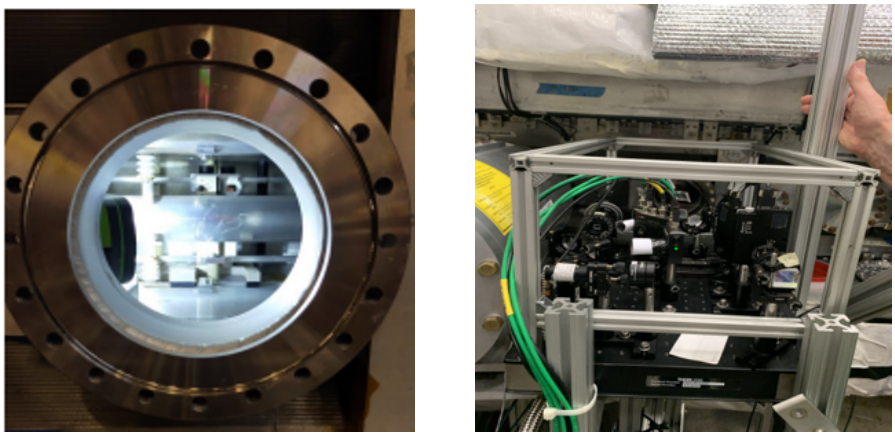

(a) Periscope system mounted in the vacuum chamber.

(b) Breadboard installed in the kicker 3 region outside the vacuum chamber.

Figure 11: Picture of periscope and breadboard after the installation.

After creating the vacuum inside the ring, the kicker 3 was powered on and controlled from the kickers' GUI. The 1.45 T-storage ring magnetic field could not be turned on, so all the measures were taken in absence of it, as a consequence no Volt-Gauss calibration was performed.
The most difficult part of the work was the laser alignment into the periscopes and into the diodes. Directing the laser using the mirrors and focusing it with the lens needs a huge precision and even a few millimeters make a difference.
After the laser was aligned the breadboard was covered with a black panel to avoid external interference and/or unexpected reflections.
The Data Acquisition system was installed on the laptop connected to the oscilloscope. The oscilloscope used was a Picoscope 7 model, connected to the laptop with an usb-port and the software used on the laptop was "Picoscope 7 T and M". The HWP were rotated by a "Thorlabs" software installed on the laptop.

In Figure 12 an example of the full kick data acquisition is shown.

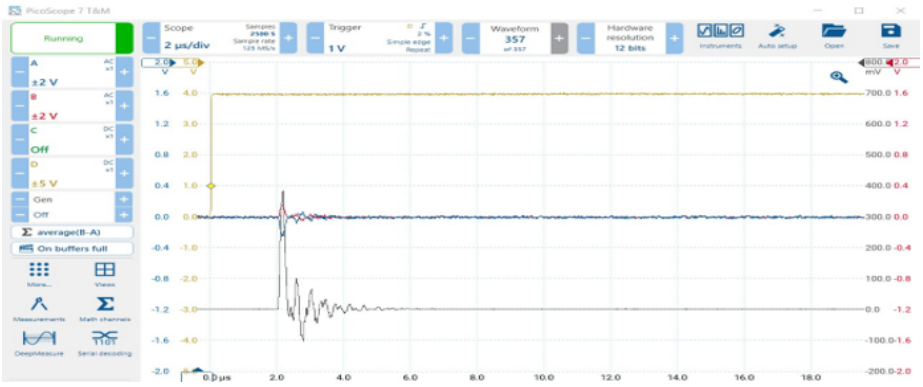

Figure 12: Picoscope configuration for main kick data acquisition.

The trigger that simulated the same pattern shown in Figure 4 was external and connected as input to a pulse generator that provided as output a pulse of 100 μs width. The pulse generator output signal was then connected to the D channel of the Picoscope and used as trigger for the acquisition. The pulse generator was fundamental also to acquire each of all the 8 different kicks in the train one at the time. In fact by modifying the delay from the generator it was possible to change the data-acquisition window, hence, which kick to acquire.

Figure 13: Picture of the pulse generator with, as example, the settings to acquire the first kick of the train of 8.

6 Main Kick Analysis

The Picoscope settings used for the full kick data acquisition were:

- 20 μs time interval
- 12 bit hardware resolution
- 512 waveform
- 4 ns sampling step

The Pulse generator delay settings to acquire each kick were:

- Kick1: 25090000 ns
- Kick2: 35089600 ns
- Kick3: 45089200 ns
- Kick4: 55088800 ns
- Kick5: 65087600 ns
- Kick6: 75087200 ns
- Kick7: 85086800 ns
- Kick8: 95086400 ns

The data acquired with this configuration were plot and analyzed using a pyROOT script and this analysis was performed in both R_0 and R_1 configuration. In the following paragraph these analyses will be described.

6.1 Main Kick R_0 analysis

Figure 15 shows the waveform of each of the 8 kicks acquired with the periscope in R_0. Each plot represent the average of the pulses acquired in about 1 hour, during the analysis I aligned the kicks to have the peak in $t = 0\,\mu$s and I subtracted the baseline offset using the average of the signal acquired in the time-interval (-5,0) μs.

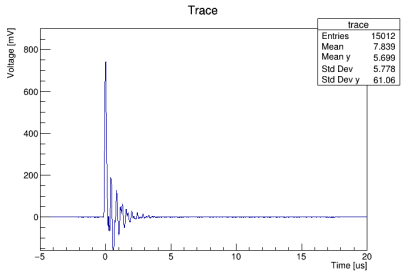

(a) Kick 1

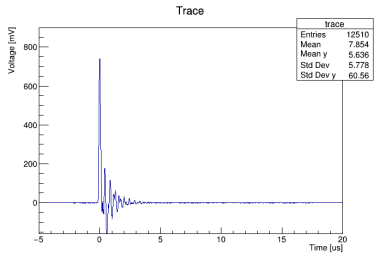

(b) Kick 2

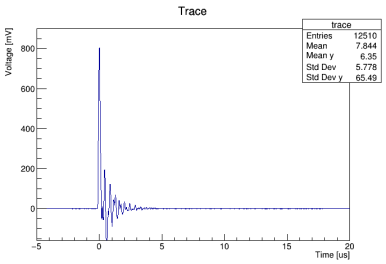

(c) Kick 3

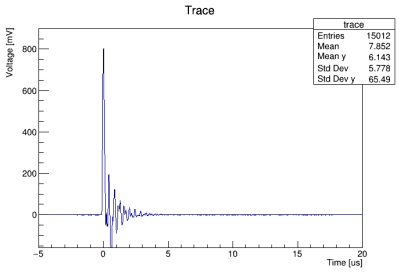

(d) Kick 4

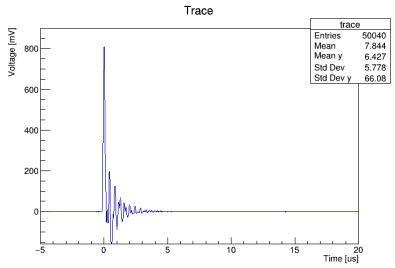

(e) Kick 5

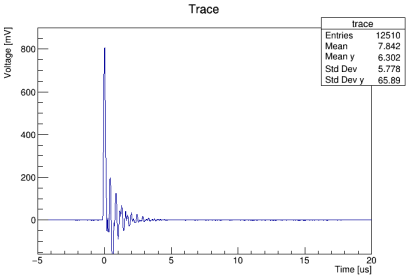

(f) Kick 6

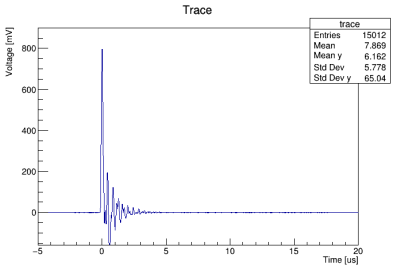

(g) Kick 7

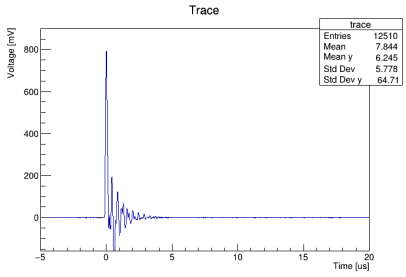

(h) Kick 8

Figure 14: Pulses acquired using the periscope positioned at R_0.

To compare the various kicks I then plotted all of them in the same canvas and I analyzed the peak and the shape differences.

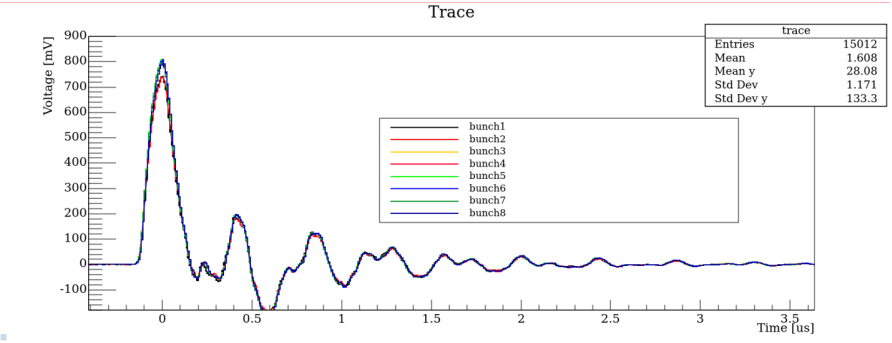

Figure 15: Comparison of the 8 kicks with the periscope position R_0.

As it is possible to see from Figure 16 the first two kicks have a lower amplitude than the other ones of a $\sim 10\%$. This effect was surprising and we decided to look if was correlated with the time the data were acquired by making a "time analysis" of the first kick and comparing it with the same procedure but applied to the fifth kick.

6.2 Investigation of kick 1 and 2 lower Amplitude in the R_0 configuration

In order to understand the reason why the first 2 kicks have a lower amplitude than the other ones an analysis on how the amplitude of the kick varies with time was performed. The full 45 min kick1 dataset was divided into three 15 min data taking subsets. For each subset was computed the average of the pulses collected and then the three final pulses were plotted in the same canvas for comparison as shown in Figure 16.

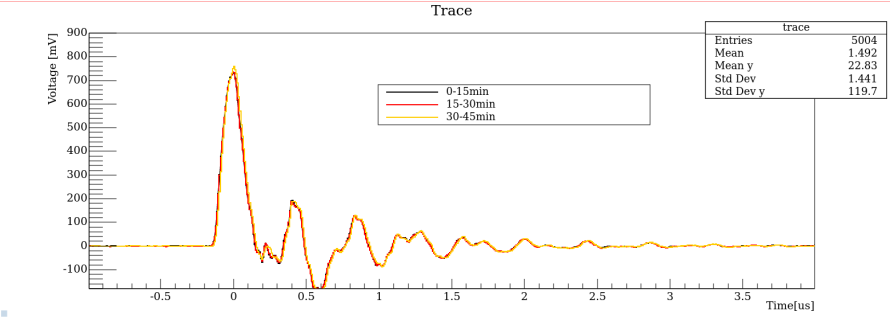

Figure 16: Comparison of the pulses from the kick1 acquired with the R_0 configuration in different time intervals (see section 6.2 for a detailed explanation).

The comparison shows that there was a change of the pulse amplitude (in the first 30 minutes the pulse amplitude is lower, black and red lines, than in the last 15 minutes, yellow line) in the time interval the data was collected. The reason of the shift may probably be explained with the kicker "warming up time", because the measures of kick1 and kick2 were taken right after the kicker was powered on. The statistic was too low to make a definitive statement but for comparison a similar analysis was performed on the 3-hours long kick5 dataset that was taken hours after the HV ramp-up of the kicker hence outside the possible "warming up" period. The dataset was divided in 3 subsets (each 1 hour of data-taking long) and Figure 17 shows these three pulses. As it possible to see, there are no differences in the amplitude in the different time subsets.

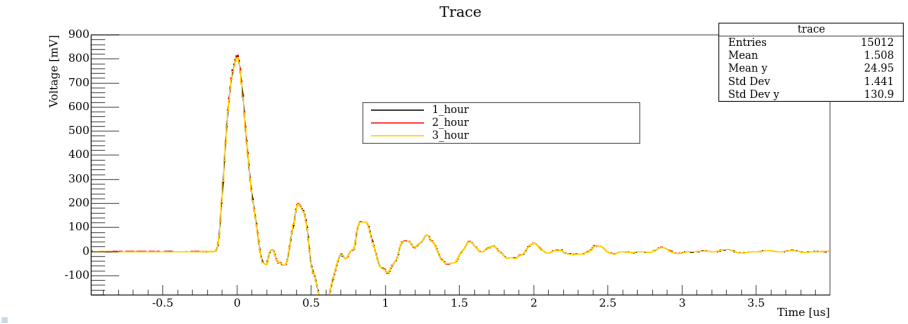

Figure 17: Comparison of the kick5 pulses from the analysis of three 1h-subsets. See text for details.

6.3 Main Kick R_1 analysis

A similar analysis was performed for the R_1 configuration. The 8 kicks plot are shown in Figure 18, and the comparison among all the kicks is shown in Figure 19.

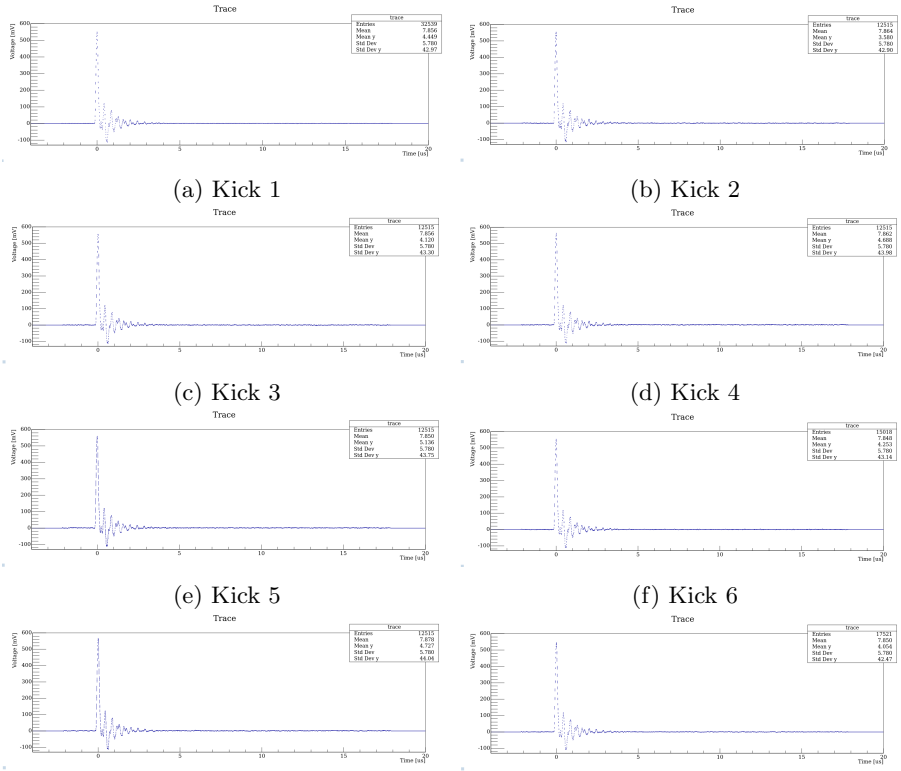

(a) Kick 1

(b) Kick 2

(c) Kick 3

(d) Kick 4

(e) Kick 5

(f) Kick 6

(g) Kick 7

(h) Kick 8

Figure 18: Pulses acquired using the periscope positioned at R_1.

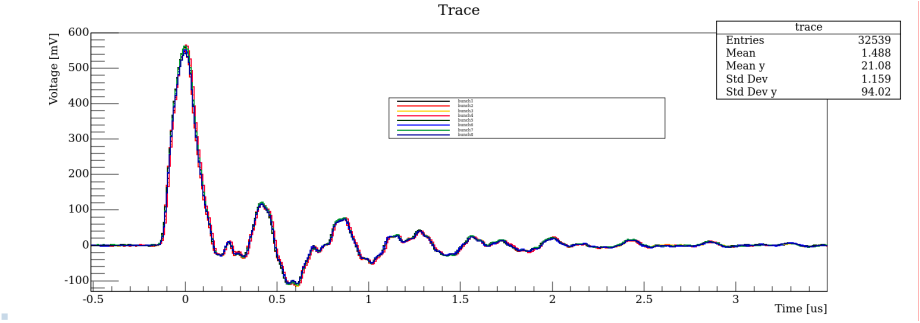

Figure 19: Comparison of the pulses from the 8 kicks acquired with the R_1 configuration

6.4 Checks performed during the setup

To understand if the experimental setup was properly installed, some checks were performed. In particular, I did a comparison between the kicks in R_0 and R_1 configurations, to check if the R_1 amplitude of the peak of the kick is lower than the R_0 one, as expected, being the R_1 periscope $\sim 1.5\,\text{cm}$ further from the center of the vacuum chamber, i.e. the position R_0.

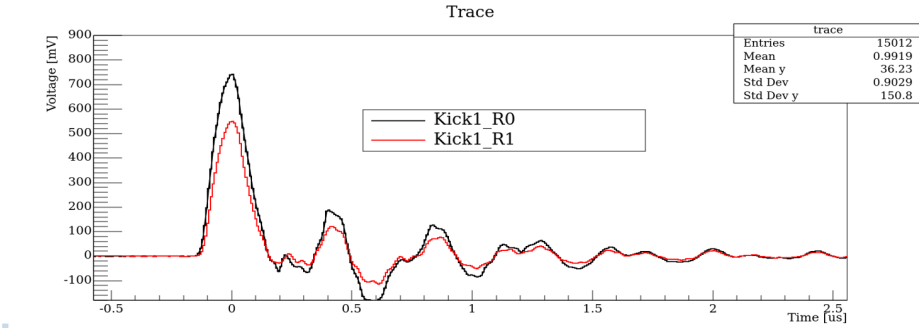

Figure 20: $R_0 - R_1$ comparison.

As shown in figure 20, R_1 peak is lower than the R_0 one and the shapes are about the same. Another check performed was testing the setup changing the impedance of the cable connected to the oscilloscope, to optimize the diode bandwidth. In fact using an high impedance termination, the diode bandwidth could be less than the nominal 150 MHz. Figure 21 shows, as expected, that the $50\,\Omega$ configuration is exactly half than the nominal one.

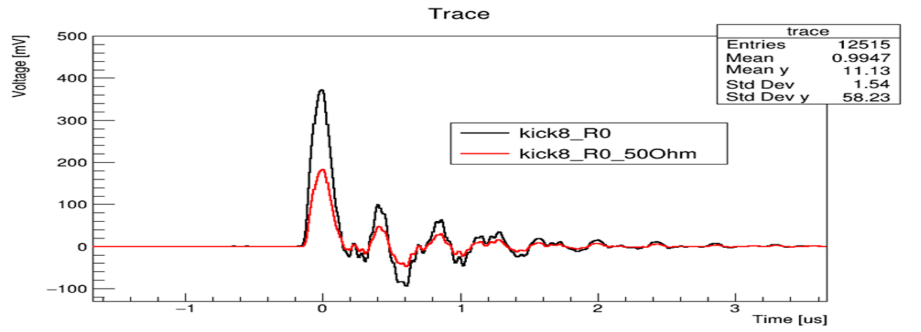

Figure 21: $50\,\Omega$ termination check.

6.5 Comparison with the simulation

The last part of the analysis was a comparison between the kicker pulses from the R0 and R1 configuration with the kicker pulse in use by the simulation

team. This cross-check is important since the simulation uses for kicker 3 the pulse shape from a previous magnetometer measurement on the kicker 1. To check only the shape (we are not interested in the amplitude since it is an input parameter of the simulation) we normalized the kicker pulses to a maximum amplitude of 1.

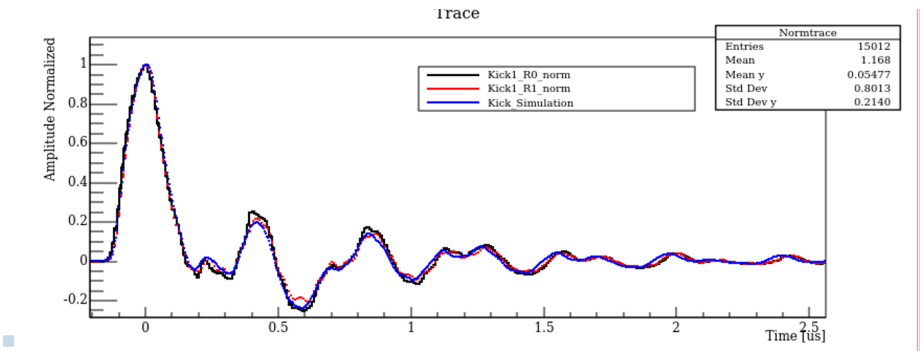

Figure 22: R_0 and R_1 kicks compared with the one used in the simulation.

As it is shown in Figure 22, both R_0 and R_1 pulses have a similar shape of the kick used in simulation which confirms the pulse used in the simulation to describe the kicker 3 kick is corrected.

7 Transient magnetic field measurement

After performing the measurement of the kicker pulse I focused on the measurement of the kickers' transient magnetic field generated by the eddy currents. In order to measure the muon anomaly we need to precisely know the anomalous precession frequency ω_a and the magnetic field experienced by the muons.

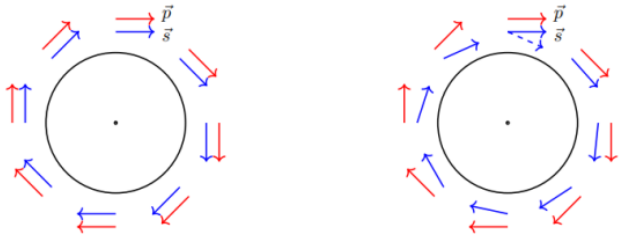

Figure 23: Illustration of the motion of the muon spin and momentum vectors for a muon orbiting in a magnetic field when $g = 2$, so the spin does not rotate relatively to the muon momentum (left), and when $g > 2$ (right).

The anomalous precession frequency of the muons inside the Muon g-2 ring is described by the equation:

$$\vec{\omega}_a = \frac{q}{m}\left(a_\mu \vec{B} - a_\mu \frac{\gamma}{\gamma+1}(\vec{\beta}\cdot\vec{B})\vec{\beta} - \left(a_\mu - \frac{1}{\gamma^2-1}\right)\frac{\vec{\beta}\times\vec{E}}{c}\right) \tag{1}$$

and it is measured in the time window between 30μs and 700μs after the muons enter the ring. Since we also need to know which magnetic field the muon see, and the eddy currents induced by the kicker pulse produce a transient field within the window in which ω_a is measured, we also need to know how it changes the main 1.45T magnetic field.

8 Eddy Currents Transient Magnetic Field Setup

The Picoscope settings used for the main kick data acquisition were:

- 195 ms time interval
- 12 bit hardware resolution
- 512 waveform
- 0.000512 ms sampling step

With respect to the previous setup we add a lens on the breadboard, as shown in the figure below, since the transient magnetic field signal is ~ 100000 times lower than the full kick, a greater focusing of the laser signal was needed.

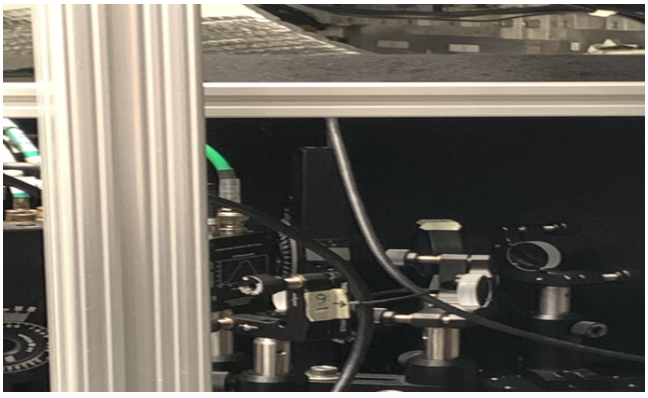

Figure 24: Breadboard with the additional lens for the kicker transient magnetic measurement.

The photo-diodes were also changed to a a photo-detector model PDB210A, that had a slower sampling rate but greater amplification, it took in input the two polarisation of the laser and gave the amplified difference between them in output.

Figure 25: Photo-detector model PDB210A (Image from Thorlabs website.

8.1 Data Analysis

The raw signals in this case were the full train of 8 pulses as can be see in Figure 26, where as before, the offset was removed by analyzing the baseline before the signal corresponding to "kick1", and then "kick1" was aligned to have its peak at $t = 0\,\mathrm{s}$.

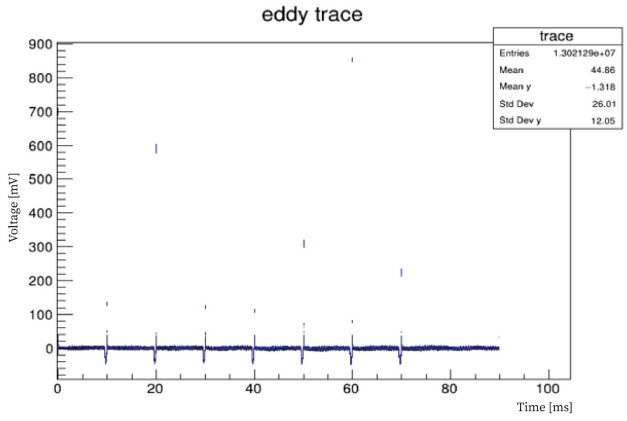

Figure 26: Example of the average of the traces acquired during $\sim 20\,\mathrm{h}$ of data-taking.

Each kick occurs every 10 ms. I therefore selected a time window of 1ms after each kick and then plotted them on the same canvas to check their alignment and compatibility.

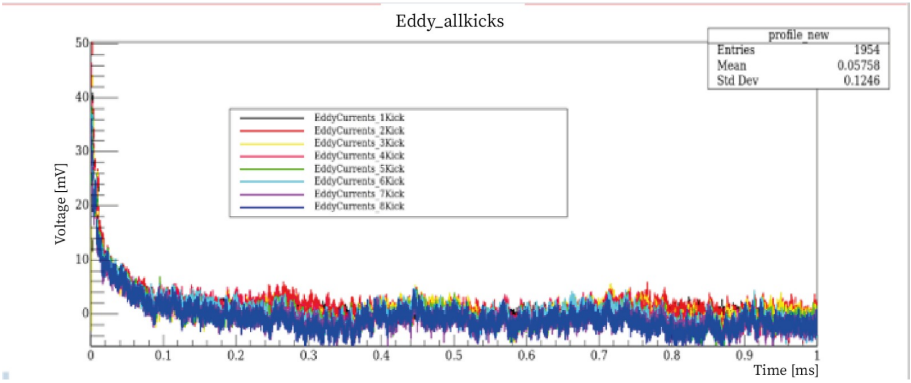

Figure 27: Eddy current effect for each of the 8 kicks in a train superimposed in the same canvas.

As shown in Figure 27, all the signals are aligned and compatible within each other. An average value of all eight signals was computed. See Figure 28.

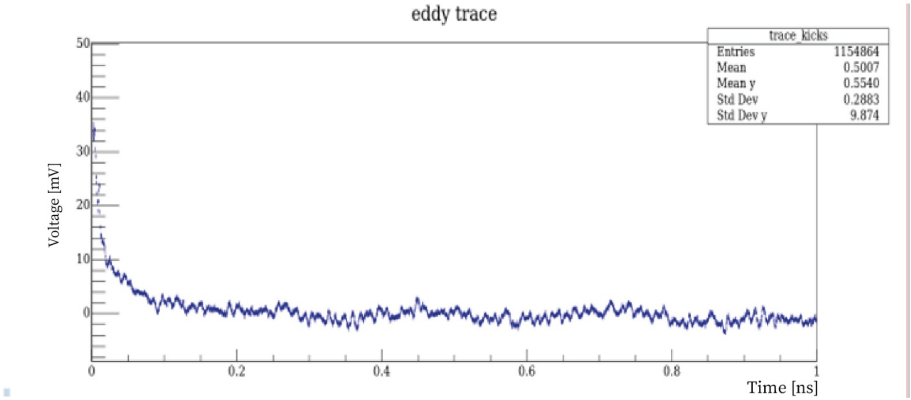

Figure 28: Measurement of the kicker transient as a average of the 8 kicks in a train in the time window 0-1ms after the kick.

8.2 Exponential fit

An exponential fit was performed on all the 8 signals to describe the eddy currents effect exponential behavior, as it is possible to see from Figure 28. The fitting function was:

$$f(x) = Ae^{\frac{-t}{\tau}} + B$$

and the fitting range was $(0.3 + k, 1 + k)$ ms where k is the kicker index included into (0, 7). The fit started at 0.3ms, as explained previously, to match the window in which the anomalous precession frequency is measured. In figure 29 all the exponential fits and the corresponding residuals FFTs for kicks from 1 to 8, are shown.

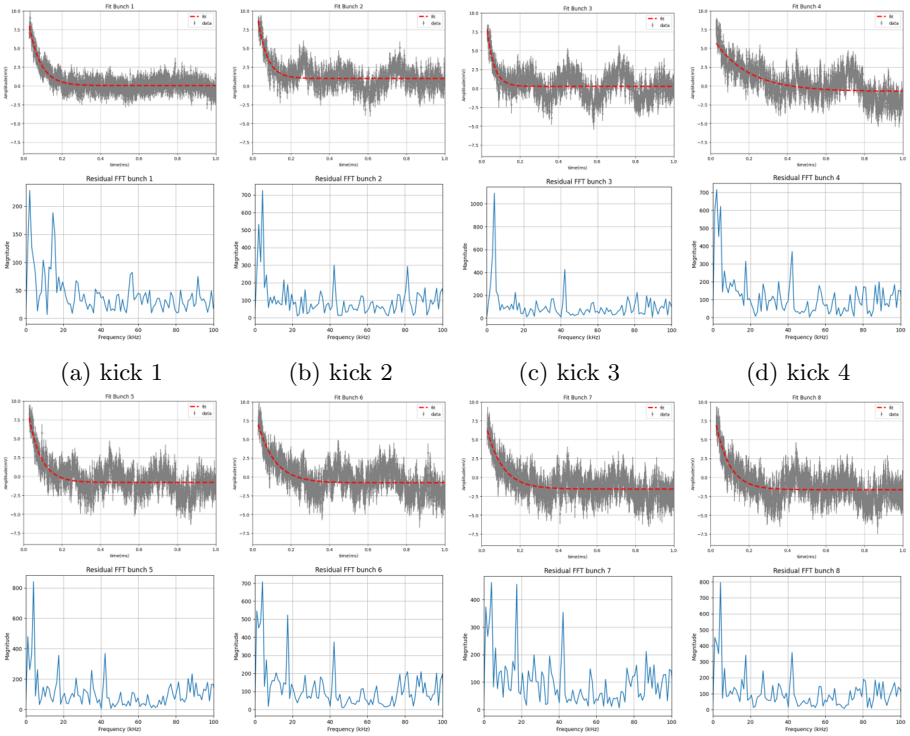

(a) kick 1 (b) kick 2 (c) kick 3 (d) kick 4

(e) kick 5 (f) kick 6 (g) kick 7 (h) kick 8

Figure 29: Exponential Fits and FFTs of the residual plots for R_1 analysis.

As can be seen in the previous plots (Fig. 29), the exponential fit is not enough to fit all the features of the signal, in fact, from the residuals FFTs distribution, it is possible to see peaks at different values of frequency, which means that it is necessary to add an oscillating component to the exponential fit function to also fit these frequencies. From the residuals FFTs plots the 3 main frequencies that are distinguishable are: $\sim 1.9\,\text{KHz}$, $\sim 3.8\,\text{KHz}$, $\sim 17\,\text{KHz}$. We think that are due to noise effects from the oscillation of the setup due to the pulses.

8.3 Noise analysis

To account for the noise effects from the oscillation, I started by adding to the fit function the 1.9 KHz frequency, which we think is generated by the

breadboard vibrations since it is seen in all the bunches. Figure 30 shows the fit using the fit function:

$$Ae^{-\frac{t}{\tau}} + B\sin(\omega_1 t + \phi)$$

with ω_1 parameter set around 1.9 KHz.

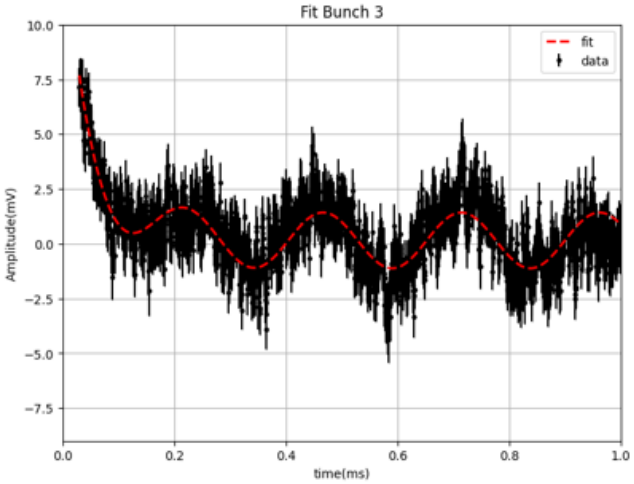

Figure 30: Signal fitted with a function that included 1.9 KHz noise frequency.

In Figure 31, the fit, after removing the frequency previously described from the data, with 3.8 KHz frequency is shown.

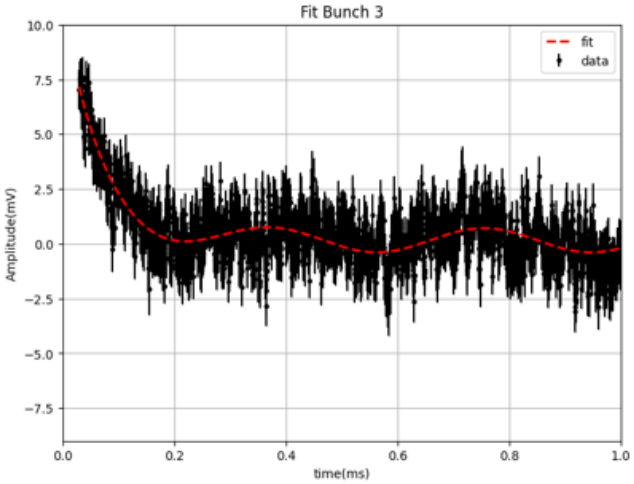

Figure 31: Signal fitted with a function 3.8 KHz noise frequency

This 3.8 KHz frequency is probably a mechanical oscillation, generated by the periscope bridge vibration, caused by the previous kick, since we do not see it in the first kick but in all the other ones.

Finally, in Figure 32, the fit, after removing the frequency previously described from the data, with 17 KHz frequency is shown.

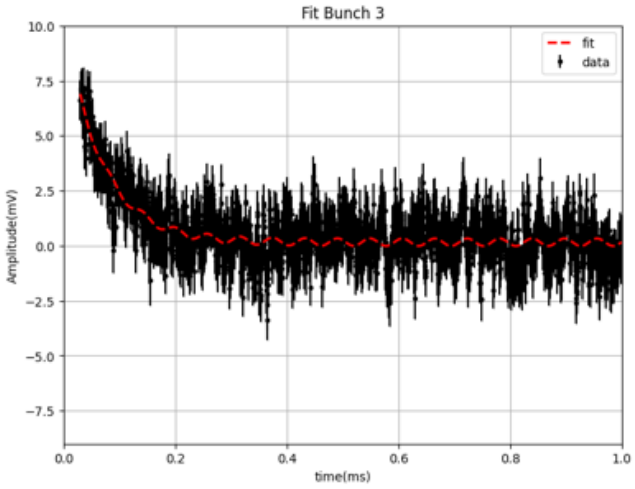

Figure 32: Signal fitted with a function 17 KHz noise frequency.

Since it is also seen by the other magnetometer team with a fiber magnetometer, we think that the 17 KHz frequency is a field oscillation, that needs to be accounted for magnetic field. Further investigation about the cause of this frequency is ongoing.

8.4 Final Fits and Results

In this section, the final fits computed on the data acquired during my internship are presented. The fitting function used is:

$$Ae^{(-t/\tau)} + B\sin(\omega t + \phi) + C\sin(\omega_2 t + \phi_2) + D\sin(\omega_3 t + \phi_3) + E$$

where ω, ω_2, ω_3 , are fixed to the frequencies described above.

From Figure 33, it can be seen that this function fits well the data and there are only small oscillations in the residual plots. The numerical result of each free parameter of the fit functions are reported below.

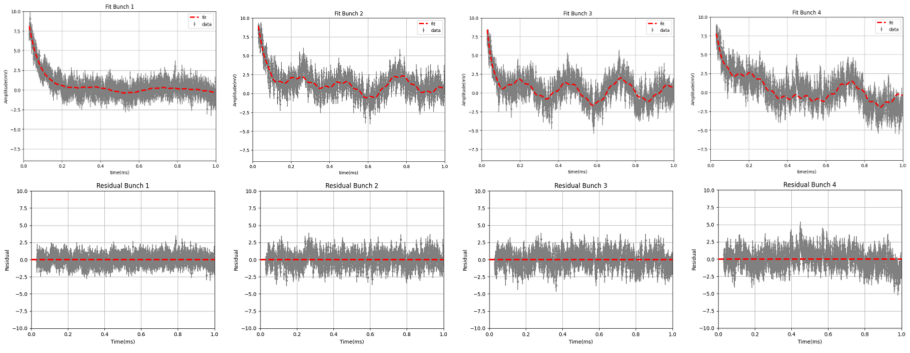

(a) Kick1 (b) Kick2 (c) Kick3 (d) Kick4

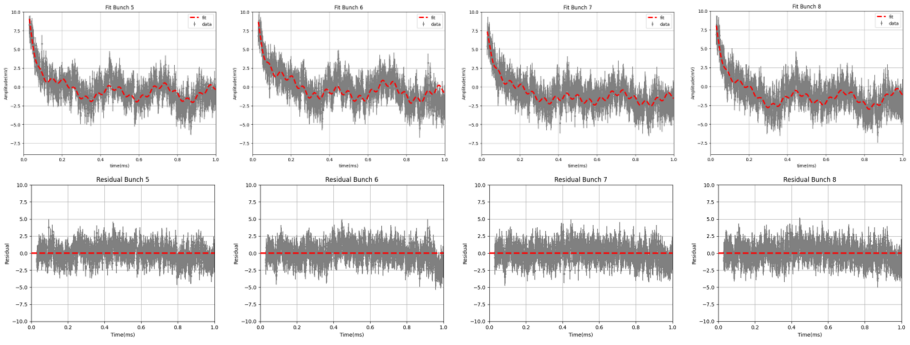

(e) Kick5 (f) Kick6 (g) Kick7 (h) Kick8

Figure 33: Final Fits and residual plots for R_1 periscope position.

In Figure 34 the results obtained for the parameters A (the exponential amplitude in mV) and τ (exponential time decay constant) are shown.

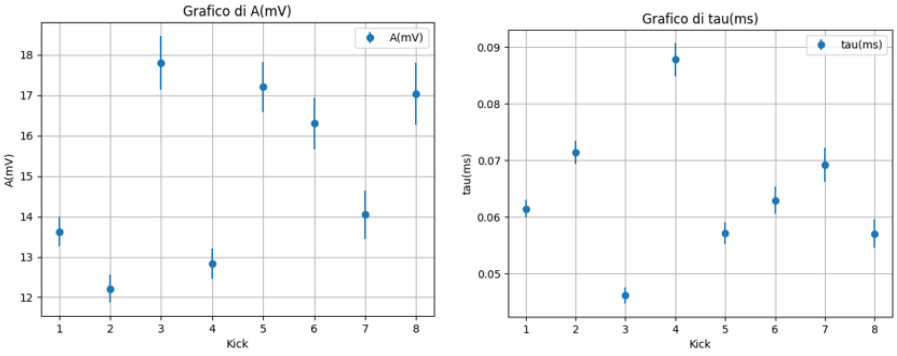

(a) Results for A (mV). (b) Results for τ (ms).

Figure 34: Fit results for each kick.

The τ parameter is lower by $\sim 20\%$ for kick 3 and higher by $\sim 30\%$ for kick 4. due to a correlation between τ and A, so the fitting function and the fitting parameters need to be optimized.
The reduced chi squared for each fit is shown in Figure 35. For the second kick is higher than the other ones, we think because of the correlation between the phases of the sinusoidal functions and the exponential τ and A parameters.

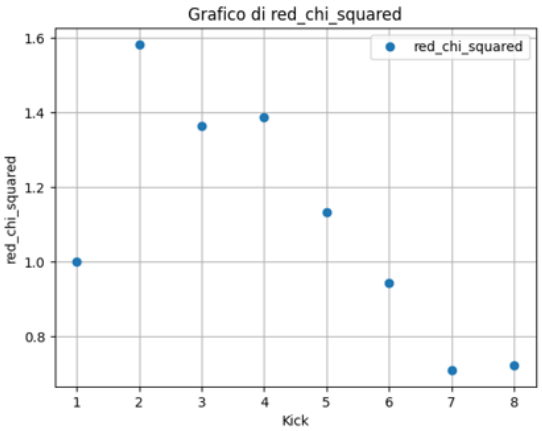

Figure 35: Results for the reduced chi squared.

The analysis was performed also on the average of the 8 kicks and the fit result is shown in Figure 36:

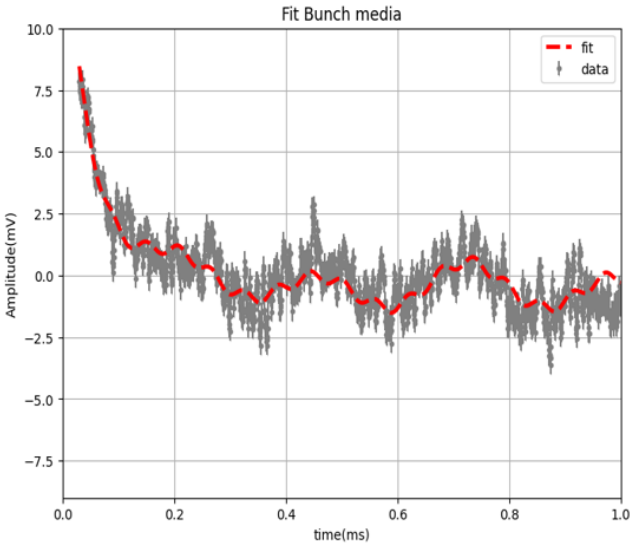

Figure 36: Total fit on average kick.

The parameters of this fit are compared with the previous results in Figure 37, where the average of the kicks is shown as kicker 9.

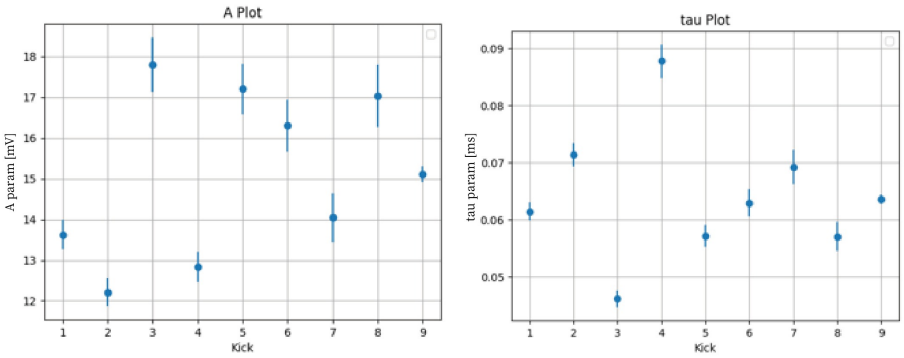

(a) Results for A (mV). (b) Results for τ (ms).

Figure 37: Results parameters on the eight kicks and on the average kick (labelled as kick 9 in the plot).

The numerical results for the average kick (figure 37) are:
$A = (15.1 \pm 0.2)\,\text{mV}$
$\tau = (0.0635 \pm 0.0007)\,\text{ms}$.
From these numbers, after performing a calibration in order to express the amplitude A in Gauss will be possible to extract the kicker transient field due to the kicker pulse.

9 Conclusion

During my internship I measured the amplitude and the shape of kicker pulses in the Muon g-2 experiment. The measurement was performed at two different radii (R_0 and R_1 configurations) and compared with a previous measurement that was used as input for the simulation. One interesting thing that I noticed was lower amplitude of same kicks possibly because the data were taken during the kicker warming time. More measurement to investigate this are needed. The second part of my work focused on the eddy currents transient magnetic field. After collecting the data I performed a fit trying to describe all the features. Results of the fit improved taking into account three noise effects. The analysis was performed only in the R_1 configuration data, but it will also be done in R_0 configuration to make a comparison of the results. Moreover there is still space for an optimization of the fit by understanding how to "de-correlate" the parameters of the fitting function (in particular $A, \tau, \phi, \phi_2, \phi_3$). Another possible approach is to test a different fitting function such as:

$$Ae^{-\frac{x}{\tau}} + Be^{-\frac{x}{\tau_2}} \sin(wx + \phi) + C\sin(w_2 x + \phi_2) + D\sin(w_3 x + \phi_3) + E$$

, where the 17 KHz frequency sinusoidal function is multiplied for a decaying exponential.

10 Future Plans

The INFN magnetometer team plans a new measurement campaign starting at the beginning of october 2023. The plan is to use also a quadrant photodiode for the eddy currents measurement to study the noise due to mechanical vibrations. They will also be able to ramp up the main magnetic field and make a calibration to express the final measurements in Gauss.

11 Acknowledgments

I enjoyed being at Fermilab really much, I could learn a lot of things working on both hardware and software parts in a physical measurement. I really enjoyed working at g-2 experiment with the magnetometer team and the possibility to spend time and talk with a lot of researchers that left me important things for my career and my personal life. A special thanks goes to my supervisors: Anna Driutti, Alberto Lusiani, Marco Incagli. A would like to say thank you also to Paolo Girotti, Renee Fatemi, Lorenzo Cotrozzi, the simulation and magnetometer team, Hogan Nguyen and the Ops team in MC1 for all the help given.

References

[1] A.P. Schreckenberger et al., "The fast non-ferric kicker system for the Muon g-2 Experiment at Fermilab," Nuclear Inst. and Methods in Physics Research A, 1011 (2021), 165597.

[2] T. Albahri et al., "Magnetic-field measurement and analysis for the Muon g-2 Experiment at Fermilab," Physical Review A, 103, 042208 (2021).